Few-Layered Boron Nitride Nanosheets for Strengthening Polyurethane Hydrogels

Feng Liu [†,‡], Rui Han [†,‡], Sina Naficy [§], Gilberto Casillas [¦], Xudong Sun [¶,*], Zhenguo Huang [‡,#,*]

[†] Key Laboratory for Anisotropy and Texture of Materials (Ministry of Education), Northeastern University, Shenyang 110819, China

‡ School of Civil & Environmental Engineering, University of Technology Sydney, Sydney, NSW 2007, Australia

§ School of Chemical and Biomolecular Engineering, The University of Sydney, Sydney, NSW 2006, Australia

¦ Electron Microscopy Centre, University of Wollongong, Wollongong, New South Wales 2500, Australia

¶ Foshan Graduate School of Northeastern University, Foshan, 528311, China

Centre for Green Technology, University of Technology Sydney, Sydney, NSW 2007, Australia

*E-mail: xdsun@mail.neu.edu.cn (X. Sun); zhenguo.huang@uts.edu.au (Z. Huang).

Abstract: Two-dimensional (2D) hexagonal boron nitride nanosheets (BNNS) is an outstanding filler and additives, since it is transparent, thermally stable, and chemically inert. However, it is difficult to obtain few-layered BNNS with large lateral sizes in an efficient way due to the strong inter-layer interactions in h-BN. Herein, a facile and efficient molten salt assisted synthesis has been developed to prepare few-layered BNNS with a few microns in lateral size. Ammonia borane was mixed with KCl and NaCl and then heated to 1000 ℃ and held for two minutes, and the resultant powders were sonicated in water to produce hydroxylated BNNS. Used as an additive with 0.066 wt% loading, the functionalized BNNS can effectively improve the mechanical modulus of polyurethane (PU) hydrogel from 1635 KPa to 2776 KPa and the optical property of

the hydrogel is not compromised. The BNNS reinforced PU hydrogel with significantly improved mechanical properties can be highly useful in the application of printed electronics.

Keywords: molten salt, boron nitride, nanosheets, hydrogels, ammonia borane.

1. INTRODUCTION

Hydrogels are crosslinked hydrophilic polymer networks with tunable physicochemical properties which have been widely applied in wastewater treatment,[1] soft robotics,[2] pressure devices,[3] etc. During the formation of the hydrogel, the permanent crosslinking formed by covalent bonds as well as the reversible linkages by hydrogen bonds, ionic bonds, or chain entanglement all contribute to the mechanical strength for polymer hydrogels.[4] Among the common polymer resins, polyurethane (PU), consisting of both hard and soft segments, is often used as a starting material in graphics, printing and coating industry owing to its excellent flexibility, high tensile strength, and good adhesion.[3,5] However, certain applications such as printed electronics require hydrogels with higher mechanical properties which cannot be met by pristine polymer hydrogels.[6,7] In order to strengthen polymer hydrogels, many studies on nanocomposite hydrogels with two-dimensional (2D) nano-fillers such as graphene and hexagonal boron nitride (h-BN) nanosheets have been carried out.[8] These 2D materials have large surface areas and high mechanical strength, which is of great importance for preparing nanocomposite hydrogels with high mechanical strength.[9] Several pioneering works have stimulated the research on BNNS/polymer composites.[10-14] For example, Zhi *et al*. used different fabrication routes such as sonication, self-chemical blowing and ball milling to prepare BNNS for mechanical reinforcement of polymers.[12-14]

Compared with graphite, the stronger interlayer coupling in h-BN makes it difficult to produce few-layered BNNS using top-down approaches which are typical for graphene preparation.

To date, BNNS has been produced via methods such as sonication-assisted exfoliation,[15] ball milling,[16] controlled gas exfoliation,[17] and hydrothermal exfoliation[18]. Generally, these methods suffer from low yield, long processing time, and small lateral size. Large-area mono- and few-layered BN can be obtained by chemical vapor deposition (CVD), but its applications are restrained by the low throughput, expensive metal catalysts, and tedious transfer processes.[19,20] Bottom-up syntheses of BNNS via liquid or solid-state reactions have also been reported.[21] Liquid-phase syntheses are facile, scalable, and the solvents provide atomic/molecular contacts and enable uniform heat control, as compared to dynamically restricted solid-state synthesis.[22]

At high temperatures, molten salts can be regarded as liquid reaction media in which h-BN formation takes place. For example, Gu *et al*. obtained 2D h-BN nanoplates with an average thickness of 80 nm using sodium amide and sodium fluoroborate as the reactants at 600-700 °C for 6-24 h in a LiBr melt.[23] Lei *et al*. fabricated layered BNNS and BCNO nanoparticles in a melted LiCl/KCl medium at 700 °C by using sodium borohydride and urea/guanidine as the reactants.[24] Tian *et al*. obtained atomically thin BNNS with a lateral size smaller than 200 nm in a melted KCl/NaCl mixture.[25] Melted salt as a reaction medium allows for efficient reactant dissolution, quick precipitation and rapid mass transfer.[26] The liquid reaction environment is more favorable for overcoming the energy barrier of crystal nucleation, leading to successful growth of BN nanomaterials.[27] At the same time, molten salt consisting of mobile cations and anions, can generate a strong polarizing force, which can stabilize ionic or covalent bonds through solvent interaction.[28,29] In spite of these advantages, the syntheses of BNNS oftentimes involve toxic reactants and/or time-consuming reactions, and generate BNNS with small lateral sizes. The choice of precursors can have a decisive impact on the morphologies and lateral sizes of the final products. Common precursors such as boric acid and melamine tend to introduce carbon impurities

and cause uncontrolled morphology.[30,31] Herein, an efficient way of synthesizing neat few-layered BNNS with large lateral size is demonstrated to tackle the aforementioned drawbacks. Ammonia borane (AB) consisting of only B, N and H elements was selected as the sole precursor, which eliminates carbon-based impurities originated from starting materials. The dehydrogenation of AB and concurrent polymerization in molten salt are believed to be beneficial for the quick formation of BNNS.[13]

In this work, few-layered BNNS was firstly prepared and then functionalized through sonication in water. Used as an additive, the hydroxylated-BN nanosheet (OH-BNNS) dramatically improved the mechanical strength of PU hydrogel. Hydrogen bonds formed between PU and OH-BNNS provide additional crosslinking, sufficient enough to significantly enhance the Young's modulus of BN/PU hydrogels even at small OH-BNNS loadings.

2. EXPERIMENTAL SECTION

2.1 Synthesis of few-layered BNNS

In a typical experiment, 100 mg ammonia borane (AB: NH_3BH_3, 98%, United Boron) was firstly ground with a certain amount of potassium chloride (Sigma-Aldrich) and sodium chloride (Sigma-Aldrich) salts, with the molar ratio between KCl and NaCl being 1:1. The mixture was then placed in a covered alumina boat and heated to 1000 ℃ at 10 ℃ min^{-1} and held for 2 minutes under Ar gas flow (150 sccm) in a tube furnace. After the heat treatment, the resulting products were washed using deionized water to remove salts. According to the weight ratio between the salts and AB, the prepared products are denoted as BNX, i.e., BN0, BN10, BN20, BN40, and BN80. For example, BN80 is derived from the mixture of 100 mg AB and 8000 mg salts. More experimental details are in the supporting information.

2.2 Fabrication of BNNS/Polyurethane Hydrogels

To functionalize and disperse the as-synthesized BNNS in water, sonication treatment was performed on a Vibra-Cell™ ultrasonic liquid processor (VCX-500). Typically, 300 mg BNNS was sonicated in deionized water (200 mL) for 1 h with a 40% amplitude. The resulting suspension was centrifuged at 3000 relative centrifugal force for 15 min, and the supernatant was then collected and dried in a vacuum oven at 80 °C. The resultant hydroxylated BNNS (OH-BNNS) was dispersed in ethanol forming a milky suspension. The concentration of saturated suspension was measured by weighing the mass of dried flakes, confirmed as 0.175 mg/L.

To prepare OH-BNNS/polyurethane hydrogels with varied concentrations of OH-BNNS, different volumes of the OH-BNNS suspension (i.e., 10, 15, 20, 25, 30, 35, 40 mL) were added to a 95:5 mixture of ethanol: water, reaching total volume of 40 mL. The concentration of OH-BNNS in the resulting suspensions was 0.044, 0.066, 0.088, 0.109, 0.131, 0.153, and 0.175 mg/L, respectively. Next, 4 g of polyether-based polyurethane composed of ethylene glycol soft segments and cyclohexylisocyanate hard segments (HydroMed D3, AdvanSource Biomaterials) was added to the OH-BNNS suspensions under continuous stirring at 40 °C for 2 days. After the polymer was fully dissolved, the samples were bath sonicated for 30 min to remove any bubbles, followed by casting in glass petri dishes. Casted samples were kept at room temperature under lids with small holes to allow slow evaporation of water and ethanol. The dried films were then submerged in water and the water was exchanged every 12 h for two days. Obtained hydrogels were stored in water at 4 °C for mechanical characterization.

2.3 Materials Characterization

X-ray diffraction (XRD) measurement was performed on a D8 Bruker Discover XRD with high-intensity Cu Kα (λ = 1.54 Å) source. Scanning electron microscopy (SEM) was conducted

on a Zeiss Supra 55VP to observe the morphology of the powders. The high-resolution imaging, electron diffraction (ED) and electron energy loss spectroscopy (EELS) analysis were carried out on a scanning transmission electron microscope (STEM) (JEOL ARM200F, operating at 200 kV). X-ray photoelectron spectroscopy (XPS) studies were performed on a PHOIBOS 100 hemispherical analyzer using Al Kα (1486.6 eV) as the X-ray source. Fourier transform infrared (FTIR) spectroscopy (Nicolet 6700 Spectrometer) was used to investigate the chemical bonds. Raman spectra were obtained at room temperature using Renishaw Raman Spectroscopy system with a laser source at 633 nm. The thickness of BNNS was characterized by atomic force microscopy (AFM, Park Systems XE7). An ultraviolet–VIS spectrophotometer (Agilent Technologies Cary 60 UV-Vis) was used to estimate the level of OH-BNNS dispersion in water. Mechanical testing was performed on fully submerged BNNS/polyurethane hydrogels using Instron Bioplus mechanical tester equipped with a temperature-controlled water bath. A 1 kN load cell was used to perform tensile mechanical testing on hydrogel films cut into 5 mm × 40 mm. Hydrogel strips were secured on wooden rods and remained fully submerged in water bath for the whole course of experiment. Tests were performed at the speed of 10 mm min^{-1} and were repeated at least five times. Swelling ratio of hydrogels was calculated by recording the mass of fully swollen hydrogels (W_s) followed by fully drying the hydrogels at 60 °C for one week and measuring the dry mass (W_d). The average swelling ratio is reported as Ws/W_d for at least five separate measurements.

RESULTS and DISCUSSION

In our method, a mixture of KCl/NaCl was used as the molten salt system to synthesize few-layered BNNS from solid ammonia borane (AB). BNNS with large lateral sizes up to 4 microns

was obtained at 1000 °C with only 2-minute dwell. AB is known to have step-wise dehydrogenation and form BNHx polymers with the value of x decreasing as the temperature increases.[13,32] As the temperature increases to 1000 °C, hydrogen is nearly completely released along with the formation of boron nitride framework.[33] As described in Figure 1a, BNHx polymeric fragments formed during dehydrogenation are well dispersed in the melted salt solvent at the elevated temperatures. The fast solvation of BNHx fragments by the ionic liquid prevents the coalesce of BN atomic layers and therefore the formation of thick BNNS. In addition, the fast mass transport in the liquid at elevated temperatures benefits the growth of the BNNS along lateral directions. Figure 1b-d and Figure S1 display the sheet-like morphology of the resulting products. With the increased weight ratio of eutectic salt to AB, the thickness of BN80 (Figure 1d, e and Figure S1e) was significantly reduced compared with other BN samples (Figure 1c and Figure S1b-d), especially with the bulk sheets of BN0 (Figure 1b and Figure S1a). This is due to the strong solvation effect of liquid salt preventing agglomeration of the BN layers. Additionally, molten salts are also beneficial for the growth of BNNS. The lateral size increases from 500 nm in BN0 to a few microns in BN80. AFM (Figure 1f) reveals that the as-prepared BN80 is of a few atomic layers thick, as shown in the line-scan profiles (Figure 1g). The BN nanosheets highlighted by the red and black lines are around 0.5 to 4 nm thick, indicating two to twelve atomic layers.

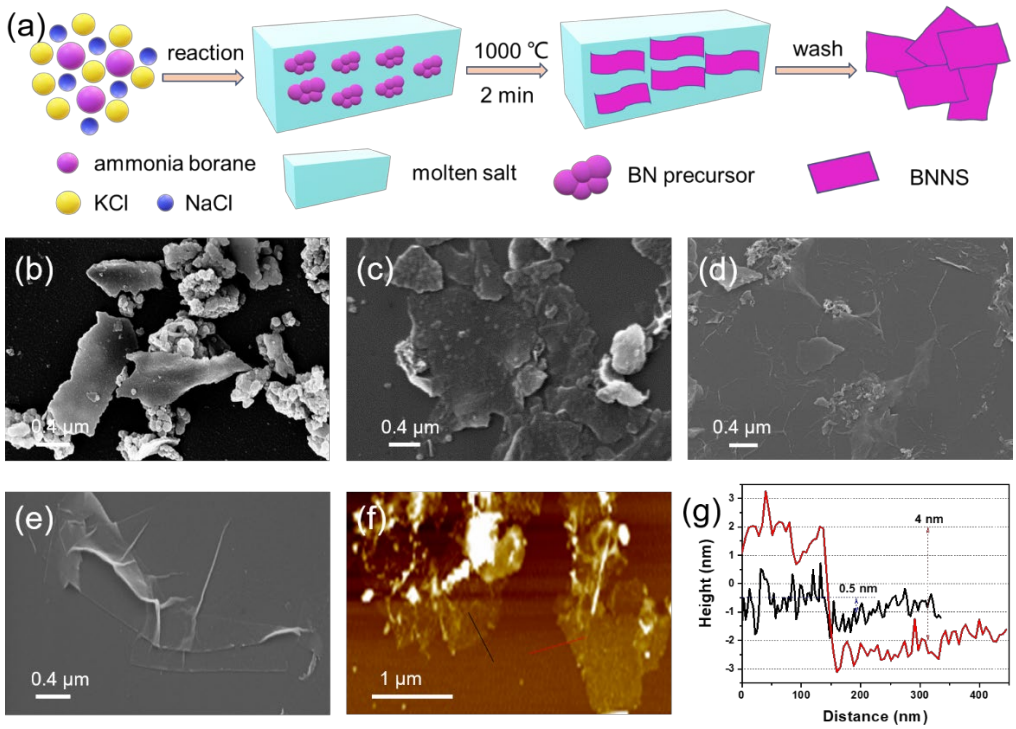

Figure 1. a) Schematic illustration of BNNS preparation; SEM images of b) BN0, c) BN40, d) and e) BN80; f) AFM image and g) corresponding line-scan profiles of BN80.

TEM image (Figure 2a) also reveals the nanosheet morphology of BN80. The electron diffraction (ED) rings (inset in Figure 2a) indicate turbostratic nature of the material.[34] HRTEM image (Figure 2b) reveals that the interlayer lattice spacing is 0.34 nm, corresponding to the 25.7-degree peak in the XRD pattern. This spacing is slightly larger than the 0.33 nm for the (002) plane of crystalline h-BN, which is due to relatively poor crystallization caused by the short dwelling time.[35] The electron diffraction pattern is in agreement with the XRD patterns (Figure 2c). There are two broad peaks located at 25.7° and 42.6°, which can be indexed to XRD pattern of h-BN.[36] The impact of temperatures (800, 900, 1000, 1100 °C) and dwell times (2 min, 1 h, 2 h and 3 h) on the BNNS morphology have been investigated. It was found that in general longer dwell and higher temperature lead to thicker sheets with slightly large later sizes. We choose 1000 °C and 2

min dwell because it is energy-efficient, and it also led to the formation of thinner nanosheets which can be effectively functionalized.

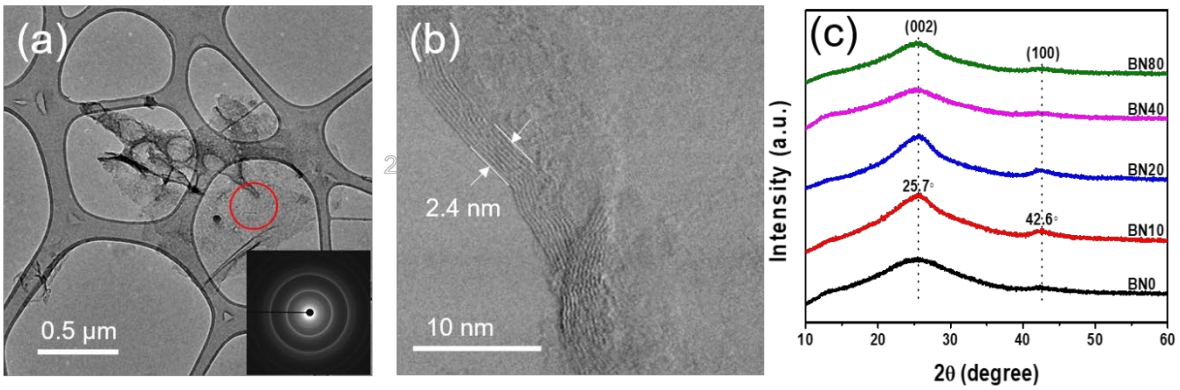

Figure 2. a) TEM image and electron diffraction pattern (inset) of BN80; b) high-resolution TEM image of BN80; c) XRD patterns of BN samples.

XPS, EELS, Raman and IR were employed to investigate the chemical structure of the as-synthesized samples. The EELS (Figure 3a) spectrum and XPS survey scan (Figure 3b) results indicate that BNNS is mainly composed of boron and nitrogen. EELS spectrum reveals the K-edge absorptions of B and N, and the core edges exhibit π* and σ* peaks, characteristic of sp^2-hybridized h-BN.[37] The XPS peaks of B 1s and N 1s (Figure 3b-d) are situated at around 188.6 and 394.6 eV, respectively. The main B 1s peak at 190.9 eV is attributed to B-N bonding, with a small shoulder at 193 eV due to B-O bond.[38] The N 1s at 398.2 eV is associated with N-B bond while the shoulder at 400.2 eV reflects the presence of N-H bonds.[39] FTIR spectra indicate that all BNNS samples have typical B-N-B bending and B-N stretching vibrations located at 798 cm^{-1} and 1371 cm^{-1}, respectively (Figure 3e).[40] For BN0, there are IR bands around 3246 cm^{-1} associated with N-H stretching, which indicates incomplete dehydrogenation within the two-minute dwell. For BNNS

obtained in molten salt, hydroxyl (-OH) groups have been introduced during the process of washing, as evidenced by the IR band at around 3422 cm^{-1}.[41,42] In the Raman spectra (Figure 3f), BN10, BN20, BN40 and BN80 all display E_{2g} peaks with FWHM values smaller than that of BN0 bulk sample, reflecting a better crystallinity of BNNS synthesized in molten salts.[37] This proves that the high temperature ionic liquid facilitates the growth and crystallization of BN nanosheets.

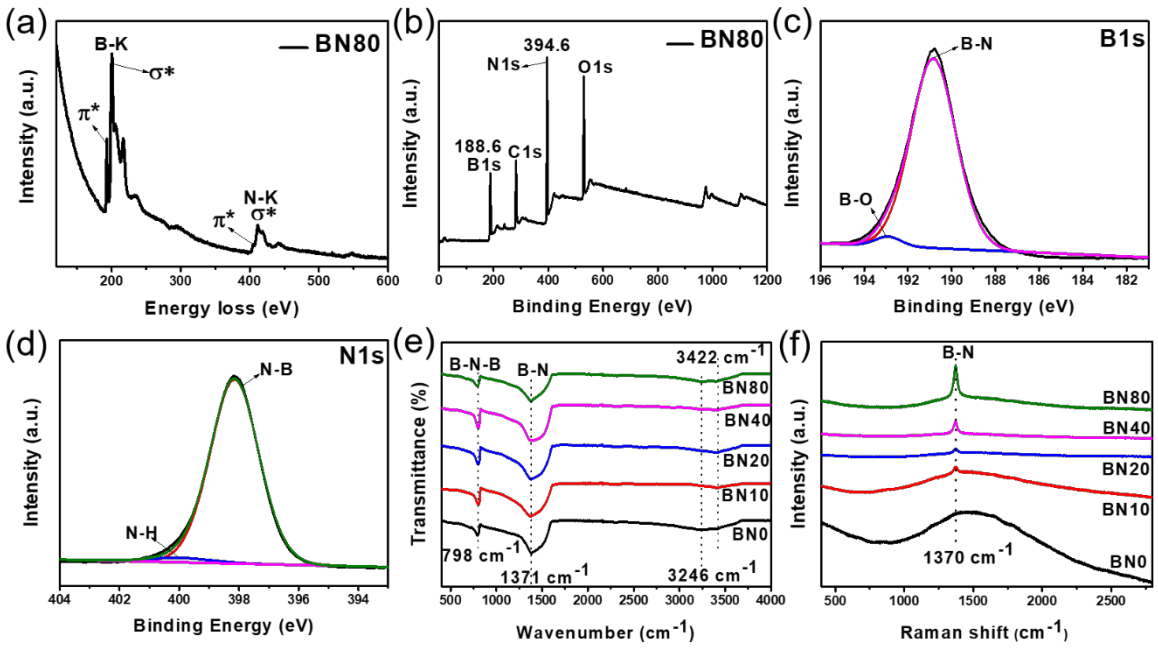

Figure 3. a) EELS spectrum, b) XPS survey scan, XPS c) B1s and d) N1s of BN80, e) FTIR and f) Raman spectra of BN samples.

The formation of sufficient hydrogen bonds between different functional groups such as -OH, C=O and N-H is crucial for unique functions of polymer hydrogels.[4,7] Hydrogen bonds also play an important role in improving mechanical strength of hydrogels.[43] Due to the hydrophobic nature of pristine h-BN, functionalization is critical for the formation of hydrogen bonds between BNNS and PU polymer. A small number of hydroxyl (-OH) groups have been introduced during the

process of washing (Figure 3 (e)), which is related to the high reactivity of sites along BNNS. To graft more OH groups on boron and make BNNS more hydrophilic,[44] sonication in water was carried out. Figure 4a reveals the change in dispersibility of the BNNS (BN80) before and after the sonication, determined by UV-vis spectroscopy. Dispersed in water, both the OH-BNNS and pristine BNNS exhibit an absorption peak at around 205 nm. But the peak intensity of OH-BNNS is much higher than that of the pristine BNNS, indicating better dispersibility enabled by the successful functionalization of the BNNS with -OH groups.[45] This good dispersibility is also evidenced by Tyndall effect (Inset in Figure 4a). A more visible FTIR band at 919 cm^{-1} associated with B-O bond (Figure 4b) confirms the functionalization of BNNS after sonication.[35] The intensity of -OH band of OH-BNNS also becomes stronger, implying a higher degree of functionalization. Figure 4c shows a 2 cm^{-1} shift of E_{2g} peak in the Raman spectrum, which is caused by reduced interlayer interactions in OH-BNNS as the result of functionalization.[46]

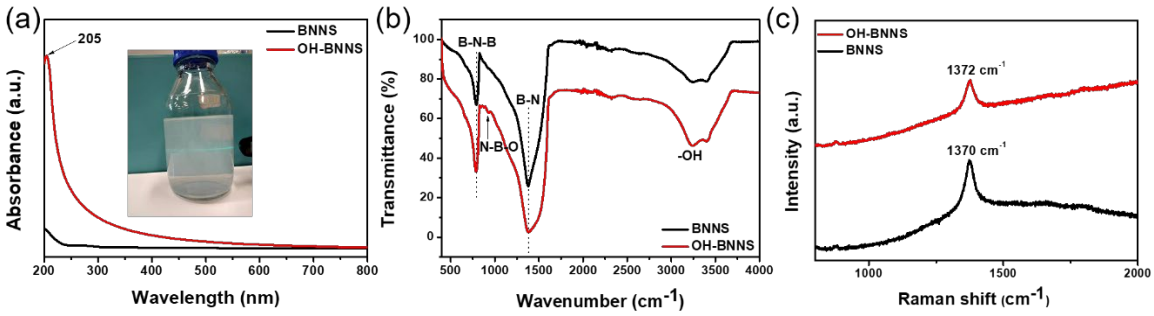

Figure 4. a) UV-vis spectra of pristine BNNS and OH-BNNS aqueous solution. Inset shows the Tyndall effect of OH-BNNS dispersion; b) FTIR and c) Raman spectra of the samples before and after sonication.

Hydroxylation allows for extensive hydrogen bonding in OH-BNNS/PU binary networks

(PUBN) hydrogel (Figure 5a). The hydrogen bonding interactions are probed by FTIR (Figure 5b). The C=O IR band of PU experienced a 15 cm^{-1} red shift after PU was mixed with OH-BNNS, which indicates the formation of hydrogen bond between C=O (proton acceptors) and -OH.[47] Due to the low loading, the vibrations of B-N itself is overwhelmed by the vibrations of functional groups in PU, such as N-H bands at 1526 cm^{-1} and C-N bands at 1241 cm^{-1}.[48] As BNNS loading increases to 10 wt% (Figure S4), B-N-B and B-N bands are detectable in the PUBN hydrogel. SEM images (Figure S5) reveal that the pristine PU hydrogels (dried at 80 °C for 24h) possess a smooth surface while the OH-BNNS/PU hydrogel shows a much rougher surface but with homogeneous features. The roughness and homogeneity indicate a uniform distribution of OH-BNNS in the PU hydrogels, likely due to the extensive hydrogen bonding interactions. Figure 5c shows that with the increase in OH-BNNS loading the modulus initially increases then decreases marginally. With 0.066 wt% OH-BNNS loading, the corresponding Young's modulus of OH-BNNS/PU hydrogel increases to its maximum value of 2776 KPa, 1.7 times higher than that of pristine PU hydrogel. OH-BNNS concentration was found to be a key factor influencing the mechanical property of PU polymer. Extensive hydrogen bonding interactions facilitate crosslinking between molecules, which allows PU hydrogels to withstand greater tensile forces. However, as the content of OH-BNNS increases, the mechanical strength of the hydrogel begins to decrease and remains at around 2200 KPa, still higher than the value of bare PU. This is probably because OH-BNNS filler interrupts the polymeric networks in the hydrogel matrix.[49] Higher OH-BNNS loading introduces more defects as can be seen from the significant agglomeration in the SEM image of dried OH-BNNS/PU hydrogel (Figure S6).[5] It should be noted that within the range of concentrations studied here the modulus of OH-BNNS/PU remains always higher than that of pristine PU while the swelling ratio (Figure 5d) remains always lower than that of pristine PU,

indicating the addition of hydrogen bonding in all formulations. For tensile tests (Figure 5e), OH-BNNS/PU hydrogel behaves better than pristine PU hydrogel even with very small amount of BNNS, indicating that the OH-BNNS acts as crosslinking components as well as reinforcing fillers in the hydrogel network. Adding such small amounts of OH-BNNS does not alter the optical appearance of the hydrogel (See Figure S7). The transmittance measurement using UV–vis spectroscopy on the OH-BNNS/PU hydrogel is shown in Figure S8. With increased OH-BNNS loading, the transmittance of OH-BNNS/PU hydrogel dropped slightly, from 90.9% transmittance of pure PU to 84.4 % of 0.066 wt% OH-BNNS/PU and 80.8% of 0.175 wt% OH-BNNS/PU at 550 nm. Compared with the opaque composite hydrogels with high loadings of OH-BNNS, the change in optical properties of samples with low loadings OH-BNNS is insignificant.

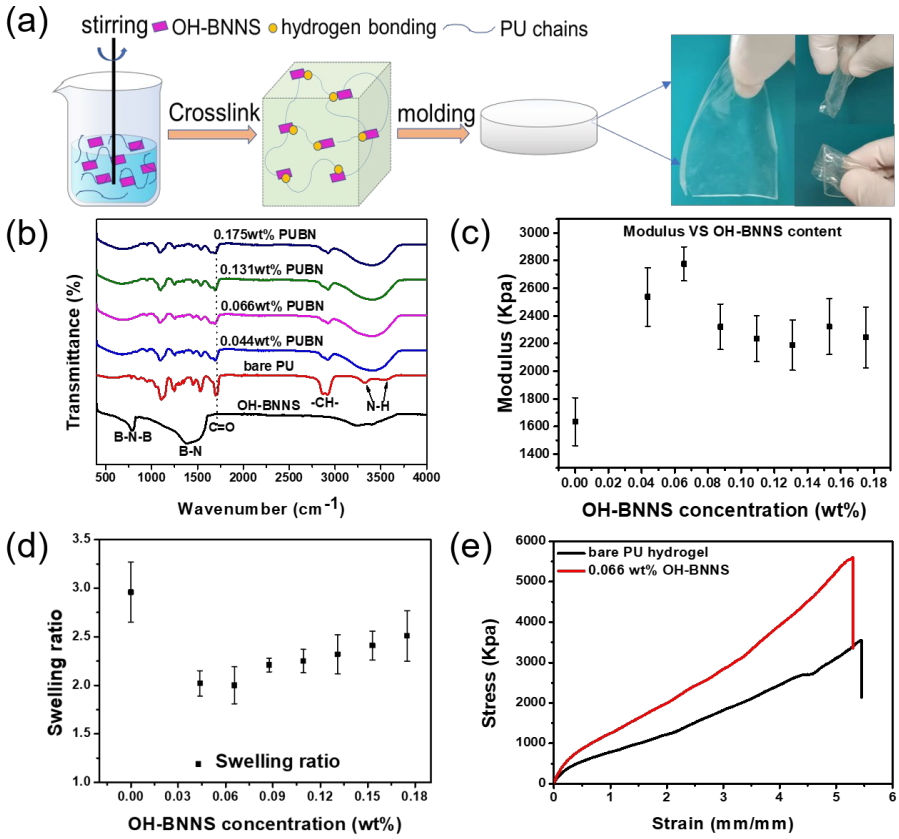

Figure 5. a) Illustration of OH-BNNS/PU hydrogel preparation; b) FTIR spectra, c) modulus curves, and d) swelling ratios of OH-BNNS/PU hydrogels; e) Mechanical stress curves of hydrogels with/without OH-BNNS.

3. CONCLUSION

Thermal decomposition of ammonia borane in molten salts at 1000 °C with two-minute dwell leads to the formation of few-layered BNNS. The dynamic ionic liquid i.e., molten salts, effectively prevents coalescence of BN atomic layers and helps to produce thin nanosheets. Rapid mass transport enabled by the liquid medium helps with the lateral growth and leads to BNNS with large lateral size. Polyurethane hydrogels mixed with hydroxylated BNNS as a reinforcing mechanical filler were successfully fabricated by a solution casting method. OH-BNNS was found to enhance the mechanic properties of PU based hydrogel via extensive hydrogen bonding interactions. The mechanical modulus of PU hydrogel increased significantly from 1635 KPa to 2776 KPa with only 0.066wt% BNNS loading, a 1.7-fold higher value than that of pristine PU hydrogel. The loading of OH-BNNS needs to be optimal since higher amounts cause agglomeration and induce more defects for stress propagation. Furthermore, there is no visible change in transparency with such low loadings. The OH-BNNS reinforced PU hydrogel with significantly enhanced mechanical property can find applications in printed electronics.

ASSOCIATED CONTENT

Supporting Information

The Supporting Information is available free of charge on the ACS Publications website at DOI: 10.1021/acsanm.xxxxxx.

SEM images of BNNS samples; FTIR spectra of BNNS/PU samples with higher BNNS loading; SEM images of PUBN hydrogel samples; Digital images of BNNS/PU with different BNNS loading; Transmittance measurement on the OH-BNNS/PU hydrogels; SEM images of BNNS products prepared at different temperatures and dwelling time.

AUTHOR INFORMATION

Corresponding Authors

*E-mail: xdsun@mail.neu.edu.cn (X. Sun);

*E-mail: zhenguo.huang@uts.edu.au (Z. Huang)

ORCID

Sina Naficy: 0000-0001-9168-6746

Zhenguo Huang: 0000-0003-1985-0884

Notes

The authors declare no competing financial interest

ACKNOWLEDGEMNT

Z.H. acknowledges financial support from the Australian Research Council's Future Fellowship (project number FT190100658).

References

(1) Huang, J.; Zhang, Z.; Weng, J.; Yu, D.; Liang, Y.; Xu, X.; Qiao, Z.; Zhang, G.; Yang, H.; Wu, X. Molecular Understanding and Design of Porous Polyurethane Hydrogels with Ultralow-Oil-

Adhesion for Oil–Water Separation. *ACS Appl. Mater. Interfaces* **2020**, *12*, 56530–56540.

(2) Xiao, F.; Naficy, S.; Casillas, G.; Khan, M. H.; Katkus, T.; Jiang, L.; Liu, H.; Li, H.; Huang, Z. Edge‐hydroxylated boron nitride nanosheets as an effective additive to improve the thermal response of hydrogels. *Adv. Mater.* **2015**, *27*, 7196-7203.

(3) Zhu, X.; Ng, L. W.; Hu, G.; Wu, T. C.; Um, D. S.; Macadam, N.; Hasan, T. Hexagonal Boron Nitride–Enhanced Optically Transparent Polymer Dielectric Inks for Printable Electronics. *Adv. Funct. Mater.* **2020**, *30*, 2002339.

(4) Chan, C. Y.; Wang, Z.; Jia, H.; Ng, P. F.; Chow, L.; Fei, B. Recent advances of hydrogel electrolytes in flexible energy storage devices. *J. Mater. Chem. A* **2021**, *9*, 2043-2069.

(5) Kim, K.; Kim, M.; Kim, J. Enhancement of the thermal and mechanical properties of a surface‐modified boron nitride–polyurethane composite. *Polym. Adv. Technol.* **2014**, *25*, 791-798.

(6) Tong, X.; Du, L.; Xu, Q. Tough, adhesive and self-healing conductive 3D network hydrogel of physically linked functionalized-boron nitride/clay/poly (N-isopropylacrylamide). *J. Mater. Chem. A* **2018**, *6*, 3091-3099.

(7) Xin, H.; Oveissi, F.; Naficy, S.; Spinks, G. M. A Sequential Debonding Fracture Model for Hydrogen‐Bonded Hydrogels. *J.Polym. Sci., Part B: Polym. Phys.* **2018**, *56*, 1287-1293.

(8) Xing, L.; Hu, C.; Zhang, Y.; Wang, X.; Shi, L.; Ran, R. A mechanically robust double-network hydrogel with high thermal responses via doping hydroxylated boron nitride nanosheets. *J. Mater. Sci.* **2019**, *54*, 3368-3382.

(9) Papageorgiou, D. G.; Li, Z.; Liu, M.; Kinloch, I. A.; Young, R. J. Mechanisms of mechanical reinforcement by graphene and carbon nanotubes in polymer nanocomposites. *Nanoscale* **2020**, *12*, 2228-2267.

(10) Meng, W.; Huang, Y.; Fu, Y.; Wang, Z.; Zhi, C. Polymer composites of boron nitride nanotubes and nanosheets. *J. Mater. Chem. C* **2014**, *2*, 10049-10061.

(11) Rasul, M. G.; Kiziltas, A.; Arfaei, B.; Shahbazian-Yassar, R. 2D boron nitride nanosheets for polymer composite materials. *npj 2D Mater. Appl.* **2021,** *5*, 1-18.

(12) Zhi, C.; Bando, Y.; Tang, C.; Kuwahara, H.; Golberg, D. Large‐scale fabrication of boron nitride nanosheets and their utilization in polymeric composites with improved thermal and mechanical properties. *Adv. Mater.* **2009**, *21*, 2889-2893.

(13) Wang, X.; Zhi, C.; Li, L.; Zeng, H.; Li, C.; Mitome, M.; Golberg, D.; Bando, Y. "Chemical blowing" of thin‐walled bubbles: high‐throughput fabrication of large‐area, few‐layered BN and Cx‐BN nanosheets. *Adv. Mater.* **2011**, *23*, 4072-4076.

(14) Wang, J.; Wu, Y.; Xue, Y.; Liu, D.; Wang, X.; Hu, X.; Bando, Y.; Lei, W. Super-compatible functional boron nitride nanosheets/polymer films with excellent mechanical properties and ultra-high thermal conductivity for thermal management. *J. Mater. Chem. C* **2018,** *6*, 1363-1369.

(15) Yi; Lin; Tiffany; V.; Williams; Tian-Bing; Xu; Wei; Cao; Hani. Aqueous Dispersions of Few-Layered and Monolayered Hexagonal Boron Nitride Nanosheets from Sonication-Assisted Hydrolysis: Critical Role of Water. *J. Phys. Chem. C* **2011**, *115*, 2679–2685.

(16) Chen, S.; Xu, R.; Liu, J.; Zou, X.; Qiu, L.; Kang, F.; Liu, B.; Cheng, H. M. Simultaneous production and functionalization of boron nitride nanosheets by sugar‐assisted mechanochemical exfoliation. *Adv. Mater.* **2019**, *31*, 1804810.

(17) Zhu, W.; Gao, X.; Li, Q.; Li, H.; Chao, Y.; Li, M.; Mahurin, S. M.; Li, H.; Zhu, H.; Dai, S. Controlled gas exfoliation of boron nitride into few‐layered nanosheets. *Angew. Chem.* **2016**, *128*, 10924-10928.

(18) Wang, N.; Yang, G.; Wang, H.; Yan, C.; Sun, R.; Wong, C.-P. A universal method for large-

yield and high-concentration exfoliation of two-dimensional hexagonal boron nitride nanosheets. *Mater. Today* **2019**, *27*, 33-42.

(19) Khan, M. H.; Liu, H. K.; Sun, X.; Yamauchi, Y.; Bando, Y.; Golberg, D.; Huang, Z. Few-atomic-layered hexagonal boron nitride: CVD growth, characterization, and applications. *Mater. Today* **2017**, *20*, 611-628.

(20) Wang, L.; Xu, X.; Zhang, L.; Qiao, R.; Wu, M.; Wang, Z.; Zhang, S.; Liang, J.; Zhang, Z.; Zhang, Z. Epitaxial growth of a 100-square-centimetre single-crystal hexagonal boron nitride monolayer on copper. *Nature* **2019**, *570*, 91-95.

(21) Wang, L.; Wang, Y.; zhang, R.; Ding, R.; Chen, X.; Lv, B. Edge Activating CO_2 Mediated Ethylbenzene Dehydrogenation by Hierarchical Porous BN catalyst. *ACS Catal.* **2020**, *10*, 6697-6706.

(22) Liu, X.; Fechler, N.; Antonietti, M. Salt melt synthesis of ceramics, semiconductors and carbon nanostructures. *Chem. Soc. Rev.* **2013**, *42*, 8237-8265.

(23) Gu, Y.; Zheng, M.; Liu, Y.; Xu, Z. Low‐Temperature Synthesis and Growth of Hexagonal Boron‐Nitride in a Lithium Bromide Melt. *J. Am. Ceram. Soc.* **2007**, *90*, 1589-1591.

(24) Lei, W.; Portehault, D.; Dimova, R.; Antonietti, M. Boron carbon nitride nanostructures from salt melts: tunable water-soluble phosphors. *J. Am. Chem. Soc.* **2011**, *133*, 7121-7127.

(25) Tian, L.; Li, J.; Liang, F.; Chang, S.; Zhang, H.; Zhang, M.; Zhang, S. Facile molten salt synthesis of atomically thin boron nitride nanosheets and their co-catalytic effect on the performance of carbon nitride photocatalyst. *J. Colloid Interface Sci.* **2019**, *536*, 664-672.

(26) Sun, J.; Chen, G.; Li, Y.; Jin, R.; Wang, Q.; Pei, J. Novel (Na, K)TaO_3 single crystal nanocubes: Molten salt synthesis, invariable energy level doping and excellent photocatalytic performance. *Energy Environ. Sci.* **2011**, *4*, 4052-4060.

(27) Liu, X.; Antonietti, M.; Giordano, C. Manipulation of phase and microstructure at nanoscale for SiC in molten salt synthesis. *Chem. Mater.* **2013**, *25*, 2021-2027.

(28) Zhang, M.; Zhou, M.; Luo, Z.; Zhang, J.; Wang, S.; Wang, X. Molten salt assisted assembly growth of atomically thin boron carbon nitride nanosheets for photocatalytic H_2 evolution. *Chem. Commun.* **2020**, *56*, 2558-2561.

(29) Luo, Z.; Fang, Y.; Zhou, M.; Wang, X. A Borocarbonitride Ceramic Aerogel for Photoredox Catalysis. *Angew. Chem.* **2019**, *58*, 6033-6037.

(30) Tzadikov, J.; Auinat, M.; Barrio, J.; Volokh, M.; Peng, G.; Gervais, C.; Ein‐Eli, Y.; Shalom, M. Layered Boron‐Nitrogen‐Carbon‐Oxygen Materials with Tunable Composition as Lithium‐Ion Battery Anodes. *ChemSusChem* **2018**, *11*, 2912-2920.

(31) Liu, F.; Han, R.; Nattestad, A.; Sun, X.; Huang, Z. Carbon-and oxygen-doped hexagonal boron nitride for degradation of organic pollutants. *Surf. Innov.* **2020**, 1-9.

(32) Huang, Z.; Autrey, T. Boron–nitrogen–hydrogen (BNH) compounds: recent developments in hydrogen storage, applications in hydrogenation and catalysis, and new syntheses. *Energy Environ. Sci.* **2012**, *5*, 9257-9268.

(33) Han, R.; Khan, M. H.; Angeloski, A.; Casillas, G.; Yoon, C. W.; Sun, X.; Huang, Z. Hexagonal Boron Nitride Nanosheets Grown via Chemical Vapor Deposition for Silver Protection. *ACS Appl. Nano Mater.* **2019**, *2*, 2830-2835.

(34) Zhong, B.; Zhang, X.; Xia, L.; Yu, Y.; Wen, G. Large-scale fabrication and utilization of novel hexagonal/turbostratic composite boron nitride nanosheets. *Mater. Des.* **2017**, *120*, 266-272.

(35) Liu, F.; Nattestad, A.; Naficy, S.; Han, R.; Casillas, G.; Angeloski, A.; Sun, X.; Huang, Z. Fluorescent Carbon‐and Oxygen‐Doped Hexagonal Boron Nitride Powders as Printing Ink for Anticounterfeit Applications. *Adv. Opt. Mater.* **2019**, *7*, 1901380.

(36) Guo, F.; Shen, X.; Zhou, J.; Liu, D.; Zheng, Q.; Yang, J.; Jia, B.; Lau, A. K.; Kim, J. K. Highly thermally conductive dielectric nanocomposites with synergistic alignments of graphene and boron nitride nanosheets. *Adv. Funct. Mater.* **2020**, *30*, 1910826.

(37) Xue, Y.; Dai, P.; Zhou, M.; Wang, X.; Pakdel, A.; Zhang, C.; Weng, Q.; Takei, T.; Fu, X.; Popov, Z. I. Multifunctional superelastic foam-like boron nitride nanotubular cellular-network architectures. *ACS Nano* **2017**, *11*, 558-568.

(38) Liu, G.; Wang, J.; Ge, Y.; Wang, Y.; Lu, S.; Zhao, Y.; Tang, Y.; Soomro, A. M.; Hong, Q.; Yang, X. Cu Nanowires Passivated with Hexagonal Boron Nitride: An Ultrastable, Selectively Transparent Conductor. *ACS Nano* **2020**, *14*, 6761-6773.

(39) Cao, Y.; Zhang, R.; Zhou, T.; Jin, S.; Huang, J.; Ye, L.; Huang, Z.; Wang, F.; Zhou, Y. B–O Bonds in Ultrathin Boron Nitride Nanosheets to Promote Photocatalytic Carbon Dioxide Conversion. *ACS Appl. Mater. Interfaces* **2020**, *12*, 9935-9943.

(40) Liu, Z.; Li, J.; Liu, X. Novel functionalized BN nanosheets/epoxy composites with advanced thermal conductivity and mechanical properties. *ACS Appl. Mater. Interfaces* **2020**, *12*, 6503-6515.

(41) Han, R.; Diao, J.; Kumar, S.; Lyalin, A.; Taketsugu, T.; Casillas, G.; Richardson, C.; Liu, F.; Yoon, C. W.; Liu, H. Boron nitride for enhanced oxidative dehydrogenation of ethylbenzene. *J. Energy Chem.* **2021**, *57*, 477-484.

(42) Weng, Q.; Wang, B.; Wang, X.; Hanagata, N.; Li, X.; Liu, D.; Wang, X.; Jiang, X.; Bando, Y.; Golberg, D. Highly water-soluble, porous, and biocompatible boron nitrides for anticancer drug delivery. *ACS Nano* **2014**, *8*, 6123-6130.

(43) Cong, H.-P.; Wang, P.; Yu, S.-H. Stretchable and self-healing graphene oxide–polymer composite hydrogels: a dual-network design. *Chem. Mater.* **2013**, *25*, 3357-3362.

(44) Kim, J.; Kwon, S.; Cho, D.-H.; Kang, B.; Kwon, H.; Kim, Y.; Park, S. O.; Jung, G. Y.; Shin,

E.; Kim, W.-G. Direct exfoliation and dispersion of two-dimensional materials in pure water via temperature control. *Nat. Commun.* **2015**, *6*, 1-9.

(45) Lee, D.; Lee, B.; Park, K. H.; Ryu, H. J.; Jeon, S.; Hong, S. H. Scalable exfoliation process for highly soluble boron nitride nanoplatelets by hydroxide-assisted ball milling. *Nano Lett.* **2015**, *15*, 1238-1244.

(46) Jing, L.; Li, H.; Tay, R. Y.; Sun, B.; Tsang, S. H.; Cometto, O.; Lin, J.; Teo, E. H. T.; Tok, A. I. Y. Biocompatible hydroxylated boron nitride nanosheets/poly (vinyl alcohol) interpenetrating hydrogels with enhanced mechanical and thermal responses. *ACS Nano* **2017**, *11*, 3742-3751.

(47) Oveissi, F.; Naficy, S.; Le, T. Y. L.; Fletcher, D. F.; Dehghani, F. Tough and processable hydrogels based on lignin and hydrophilic polyurethane. *ACS Appl. Bio Mater.* **2018**, *1*, 2073-2081.

(48) Hong, H.-J.; Kwan, S. M.; Lee, D. S.; Kim, S. M.; Kim, Y. H.; Lim, J. S.; Hwang, J. Y.; Jeong, H. S. Highly flexible and stretchable thermally conductive composite film by polyurethane supported 3D networks of boron nitride. *Compos. Sci. Technol.* **2017**, *152*, 94-100.

(49) Tavman, I. H. Thermal and mechanical properties of aluminum powder-filled high-density polyethylene composites. *J. Appl. Polym. Sci.* **1996**, *62*, 2161-2167.

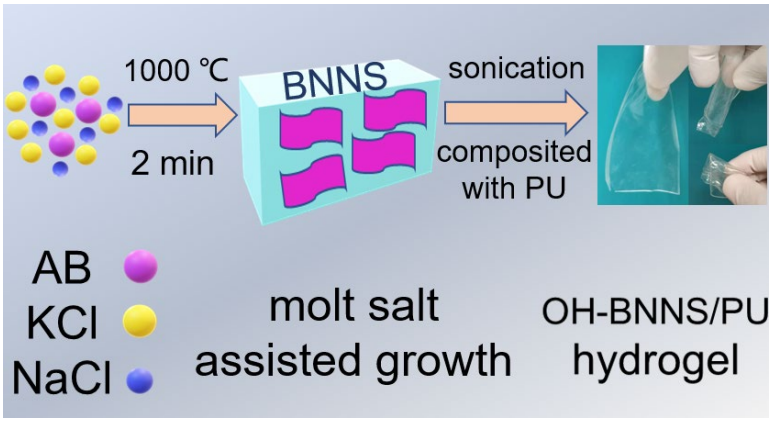

Table of Contents Graphic